

# Optical Interconnections on Electrical Boards Using Embedded Active Optoelectronic Components

Sang-Yeon Cho, Martin A. Brooke, *Member, IEEE*, and Nan Marie Jokerst, *Fellow, IEEE*

**Abstract**—Significant opportunities are emerging for optical interconnections at the board, module, and chip level if compact, low loss, high data rate optical interconnections can be integrated into these electrical interconnection systems. This paper describes an integration process for creating optical interconnections which can be integrated in a postprocessing format onto standard boards, modules, and integrated circuits. These optical interconnections utilize active thin-film optoelectronic components embedded in waveguides, which are integrated onto or into the interconnection substrate, thus providing an electrical output on the substrate from an optical interconnection. These embedded optical interconnections are reported herein using BCB (*Benzocyclobutene*) polymer optical waveguides in two different formats, as well as a third waveguide structure using a BCB cladding with an Ultem core. All of these waveguides were fabricated with InGaAs-based thin-film inverted metal–semiconductor–metal (I-MSM) photodetectors embedded in the waveguide layer, thus eliminating the need for beam turning elements at the output of the waveguide. These embedded interconnections have been fabricated and tested, and the coupling efficiency of the optical signals from the waveguides to the embedded photodetectors was estimated from these measurements. These measurement-based estimates are then compared to theoretical models of the coupling efficiency. Using the theoretical coupling efficiency model, variable coupling can be engineered into the interconnect design, thus enabling partial coupling for arrays of photodetectors embedded in waveguide interconnections.

**Index Terms**—Embedded thin-film photodetector, optical interconnection.

## I. INTRODUCTION AND MOTIVATION

AS ELECTRONIC system aggregate data rates rise and the size decreases, conventional electrical interconnections face multiple challenges at the board, module, and chip level. Tradeoffs between power consumption, area, and signal integrity (jitter, delay, skew) must be evaluated in high performance electrical interconnection systems. Both innovative architectural and design approaches, and technological innovation at the physical layer level play important roles in improving interconnection performance. For example, innovative designs, such as equalization [1] and advanced signaling techniques [2], coupled with improvements in silicon integrated circuit (Si IC) technology, have provided many of the gains in system performance to date. However, physical limitations will ultimately force technology changes at the physical layer if performance gains are to continue well into the future.

Many quantitative comparisons of interconnection performance have been published discussing electrical and optical interconnections [3]–[7], and the question of how to integrate optical interconnections into an electrical interconnection system is a topic of currently intensive study. Optical interconnect approaches include free space interconnects with diffractive optical elements [8], silicon optical bench interconnects [9], and guided wave interconnections, including substrate guided mode interconnects [10], fiber optic waveguides [11], and integrated waveguides [12]. Summary articles on this topic are available in the literature [7]. This paper will focus upon waveguide optical interconnections, which are integrated directly onto electrical interconnection package media such as boards and modules, and directly onto integrated circuits.

Electrical boards, modules, and integrated circuits are essentially planar, and thus, a planar waveguide optical interconnection scheme matches the electrical systems from a topographical standpoint. There are a variety of approaches to the partitioning of optical and electrical signals in a mixed electrical/optical interconnection system. Figs. 1(a) and 2(a) illustrate two of the basic partitioning options: 1) turn the optical beam out of the substrate into the optoelectronic active device [Fig. 1(a)]; or 2) keep the optical beam confined to the substrate, and embed the active optoelectronic device in the substrate [Fig. 2(a)]. Optical beams can be turned 90 degree using mirrors or gratings, and can be turned into either optical/optoelectronic devices [Fig. 1(a)], or onto optoelectronic integrated circuits (OEICs) [Fig. 2(a)], which may contain a combination of active and passive optical/optoelectronic devices and circuitry. By employing diffractive optical elements, such as preferential gratings, high coupling efficiency and limited spectral selectivity can be achieved [13]. As illustrated in Fig. 1(b) and (c), to emit or detect this out-coupled beam means that the active optoelectronic device must operate facing the board/module/chip, in a flip chip orientation [as shown in Fig. 1(b)] or as a flip chip OEIC [14], as shown in Fig. 1(c). Drawbacks to this approach include the alignment constraints of the optical beam and decrease in coupling efficiency as the photodetectors decrease in size with increasing data rates.

An alternative approach is to have the optical signals originate and/or terminate in the waveguide directly on the board/module/chip, without optical beam turning. Fig. 2 illustrates some of the options for embedding a detector in a waveguide, including embedding in the core [Fig. 2(d) and (e)], and in the cladding [Fig. 2(f) and (g)]. Optical interconnections with integrated waveguides and OE devices in the substrate and epilayers [12], [15]–[19] have been reported in compound semiconductors, such as InP-based materials, with reported

Manuscript received September 25, 2002; revised February 5, 2003.

The authors are with NSF Packaging Research Center, School of Electrical and Computer Engineering, Georgia Institute of Technology, Atlanta, GA 30332-0250 USA.

Digital Object Identifier 10.1109/JSTQE.2003.813324

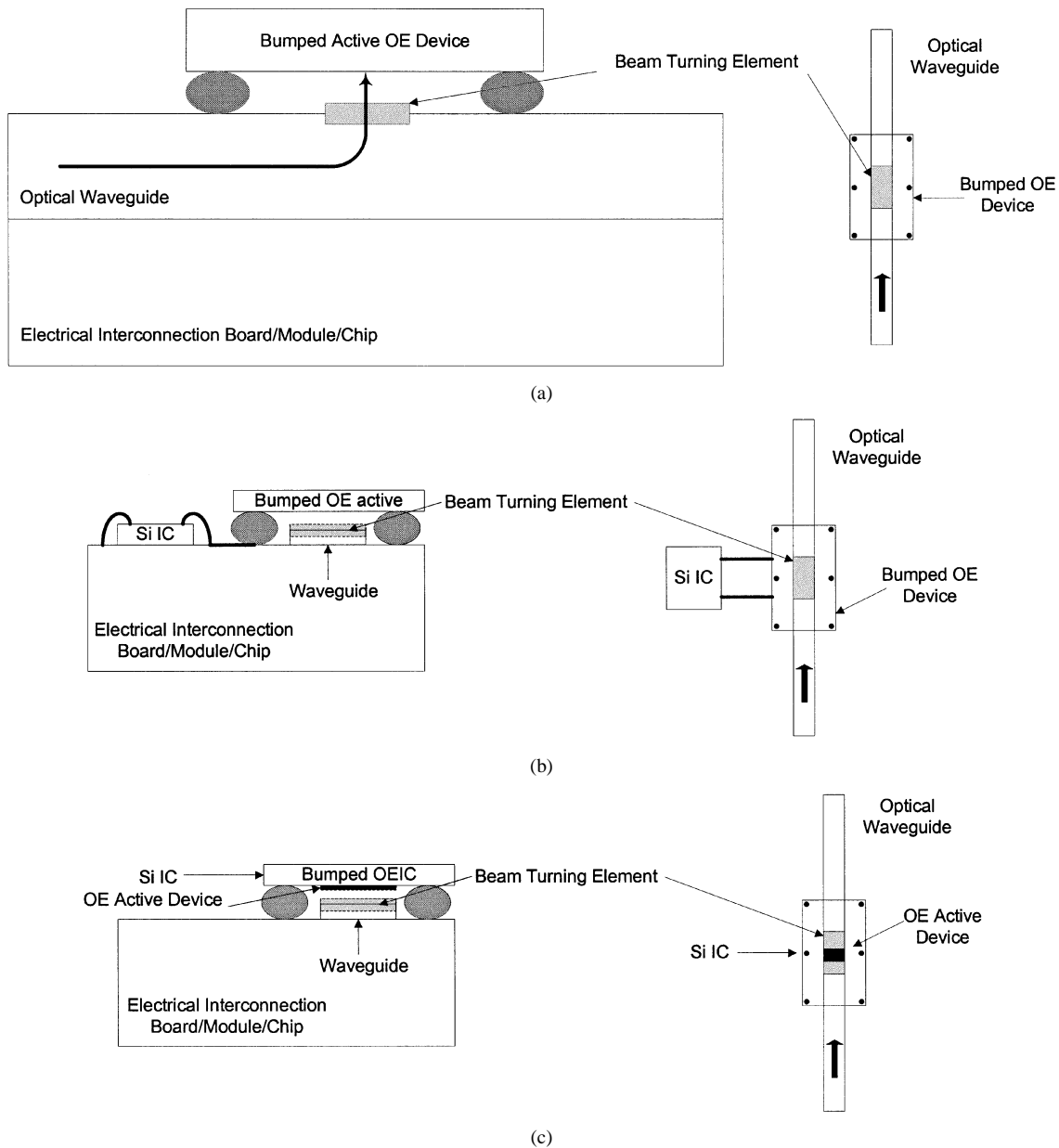


Fig. 1. Illustration of the integration of optical signal coupling in an integrated planar lightwave circuit format into an electrical interconnection system. (a) Coupling with an optical beam turning element, such as a diffractive optical element or micromirror; (b) waveguide with a beam turning element which produces a surface normal optical output beam detected by a bumped OE active device, with a Si interface integrated circuit wirebonded onto the electrical interconnection substrate; (c) waveguide with a beam turning element which produces a surface normal optical output beam detected by a bumped OEIC, with an active thin-film OE device integrated directly onto the Si interface integrated circuit.

high coupling efficiency and monolithic integration. However, the use of polymer waveguides and low cost epoxy and polymer substrates is of great interest for optical interconnections in electrical interconnection systems, and hence the particular emphasis upon polymer waveguides for low cost optical interconnection which are process compatible with current board, module, and integrated circuit technology. Polymer waveguides integrated onto Si [18] or GaAs [19], [20] electrical interconnection substrates which have photodetectors fabricated in the substrate, thus creating embedded waveguide interconnections, have been demonstrated. However, this approach does not accommodate epoxy and polymer substrates. An alternative embedded waveguide approach utilizes thin-film OE devices (with the OE device growth substrate removed), which can be

bonded to any host substrate, including polymer and epoxy boards such as FR4. The polymer waveguide material can then be deposited directly onto the thin-film active OE devices, which are thus embedded directly into the waveguide, as illustrated in Fig. 2(d) and (e), or embedded in the cladding, as in Fig. 2(f) and (g).

This embedded optoelectronic waveguide interconnection technology for OE devices gives the interconnect designer the option to create an optical interconnection on the board/module/chip which has exclusively electrical inputs and/or outputs (but can have, at the designer's option, optical inputs/outputs as well). To realize a planar optical interconnect with an embedded source, one type of optical input which can be implemented is embedded thin-film edge emitting lasers (at

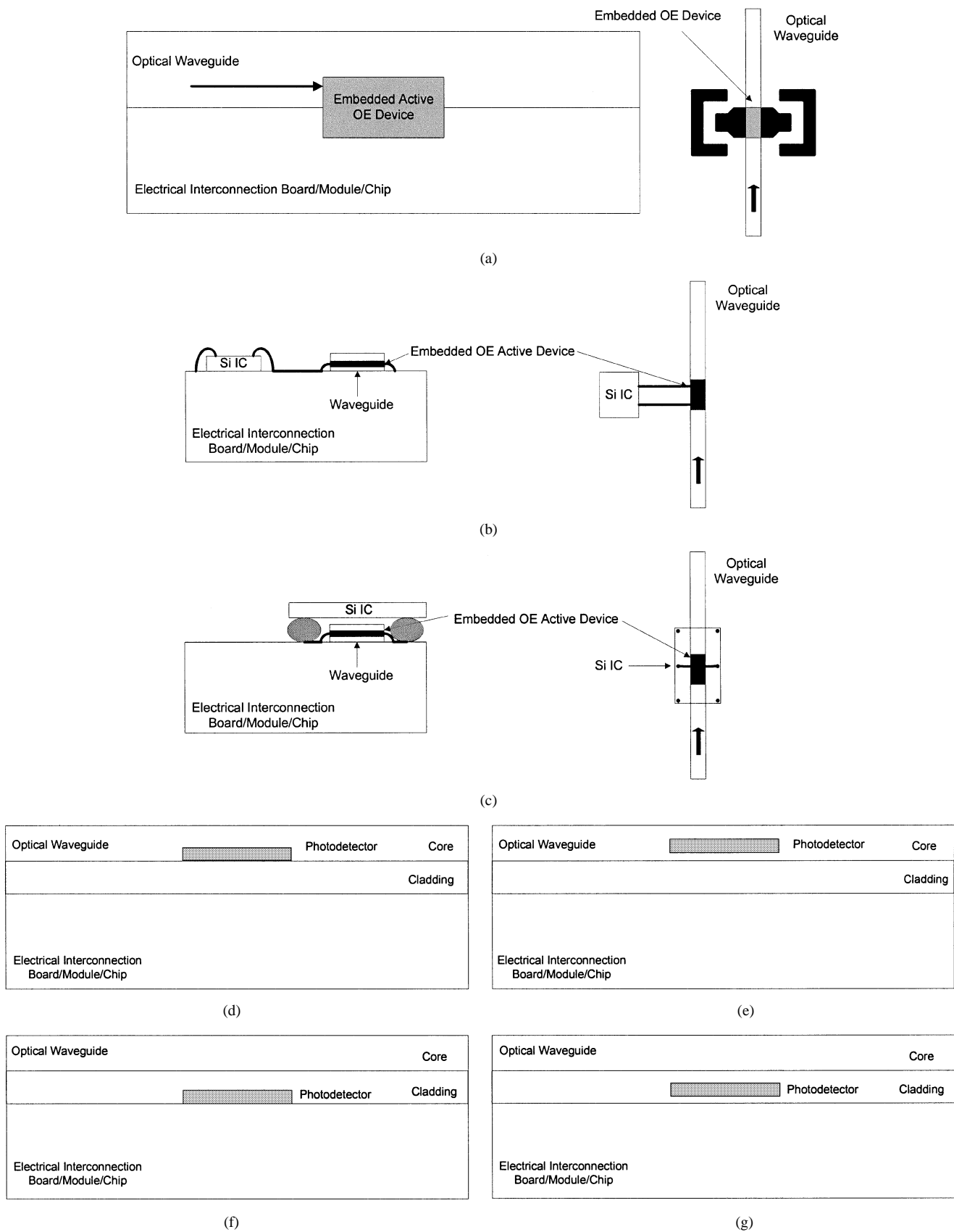


Fig. 2. Cross section and top view of optical and electrical signal routing options in integrated planar lightwave circuit interconnections with embedded active OE devices integrated into conventional electrical interconnection substrates. (a) Evanescent or direct coupling structure; (b) waveguide with an embedded photodetector which detects an input optical beam with photocurrent output to a Si interface integrated circuit which is wirebonded to the embedded PD, all located on the electrical interconnection substrate; (c) waveguide with embedded photodetector which detects an input optical beam with a photocurrent output to a Si interface integrated circuit which is bump bonded to the PD and to the electrical interconnection substrate; (d), (e), (f), (g) embedded active OE device integration options for photodetectors, which include: (d), (e) direct coupling; (f), (g) evanescent field coupling.

wavelengths including 850, 980, 1300, and 1550 nm) which emit directly into the waveguide structure. Vertical cavity surface emitting lasers as optical signal sources necessitate the use of beam turning elements (note that the embedded thin-film OE device technology described in this paper can also be applied to GaAs-based devices such as photodetectors (PDs) [21]). Implementing these types of planar lightwave circuit (PLC) optical interconnections with embedded emitters and detectors may eliminate the need for optical beam turning elements which route the beam perpendicular to the surface of the board/module/chip, and reduces waveguide to active OE device optical alignment to an assembly step with sequentially aligned masking steps, which mimics integrated circuit fabrication. In addition, the integration of additional PLC passive and further active embedded devices opens multiplexing and optical signal processing options for more complex microsystems. The electrical interface circuits can be connected directly to the embedded active OE devices, as shown in Fig. 2(b) and (c), through either wire bonding or bump bonding (as rising data rates preclude wire bonding), respectively, or through the electrical interconnection substrate lines. The assembly tradeoff that is inherent in the embedded optical waveguide interconnection is that the OE active devices are bonded directly to the substrate rather than bumped to the substrate. To minimize the impact of introducing optical interconnections into electrical interconnection substrates, the embedded OE waveguide interconnections can be integrated onto a fabricated electrical interconnection substrate through postprocessing. To enhance yield, at the board/module level, the optical interconnections can be electrically tested before chipset integration.

This paper describes the integration of independently optimized waveguides, embedded thin-film PDs, and a standard Si substrate that can be used as an interconnection substrate. The integration processes described herein are also being applied to high temperature epoxy FR4 boards. Presented herein are the integration processes and measurement results for the integration of a thin-film InGaAs PD embedded in two configurations of Benzocyclobutene (BCB) polymer waveguides integrated onto a Si interconnection substrate, as shown in Fig. 2(d) and (e), and an Ultem (core)/BCB (clad) polymer waveguide integrated onto a Si interconnection substrate, as shown in Fig. 2(f). The use of thin-film ( $\sim 1\text{-}\mu\text{m}$ -thick) PDs (with the OE device growth substrate removed) enables the PDs to be bonded and electrically connected to the Si interconnection substrate and embedded in the polymer optical waveguides. Because these PDs are embedded in the waveguide, the optical signal can be coupled from the waveguide into the PD without the use of beam turning elements. Thus, the optical signal is confined to the substrate, and electrical signals from the PD are the output. A receiver can then be wire bonded or flip chip bonded to the PD, as shown in Fig. 2(b) and (c), converting the PD output signal into a standard electrical signal. Using this technology, the thin-film OE devices, optical waveguides, and electrical interconnection media can be optimized separately for optimal mixed optical and electrical signal distribution for board, module, and chip level interconnections.

Three of the structures introduced in Fig. 2(d)–(f) have been fabricated, and the optical coupling efficiency estimated through measurement. Theoretical models of the coupling efficiency for

these different structures have also been developed, and a comparison between theory and experiment for the three structures is presented herein. Finally, these models are used to explore more optimized structures for the photodetectors used herein, and more optimal coupling efficiencies from these theoretical models are discussed.

## II. FABRICATION OF PHOTODETECTORS EMBEDDED IN WAVEGUIDES USING THREE DIFFERENT INTEGRATION STRUCTURES

Thin-film photodetectors have been embedded in three different waveguide structures, one embedded in the cladding below the waveguide, and two embedded in the waveguide core: one in the bottom of the waveguide core, and two inside the waveguide core. To implement these embedded photodetector optical interconnections, three components were integrated together to form the interconnection: the photodetector, the optical waveguide, and the interconnection substrate.

The inverted metal–semiconductor–metal (I-MSM) photodetectors were independently grown, fabricated, and subsequently bonded to the metal contact pads on the interconnection substrate. The as-grown MSM material was InP–InGaAs (2000 Å stop etch layer)– $\text{Al}_{0.48}\text{In}_{0.52}\text{As}$  (400 Å cap layer)– $\text{Al}_{0.48}\text{In}_{0.52}\text{As}$  graded to  $\text{In}_{0.53}\text{Ga}_{0.47}\text{As}$  (600 Å)– $\text{In}_{0.53}\text{Ga}_{0.47}\text{As}$  (0.74- $\mu\text{m}$ -thick absorbing layer)– $\text{In}_{0.53}\text{Ga}_{0.47}\text{As}$  graded to  $\text{Al}_{0.48}\text{In}_{0.52}\text{As}$  (600 Å)– $\text{Al}_{0.48}\text{In}_{0.52}\text{As}$  (400 Å cap layer). Interdigitated 40-Å Pt/350-Å Ti/400-Å Pt/2500-Å Au Schottky fingers 100  $\mu\text{m}$  long with 2- $\mu\text{m}$  finger width and 2- $\mu\text{m}$  finger spacing were patterned on a 100  $\mu\text{m} \times 150 \mu\text{m}$  detection area. By using the Pt diffusion barrier [22] on the MSM, the Schottky contacts are not degraded by the waveguide thermal process, and as a result, the dark current is not degraded by the waveguide integration process. Next, each MSM device was mesa etched down to the InP growth substrate using citric :  $\text{H}_2\text{O}_2$  (10 : 1). The MSM mesas were protected with Apiezon W and immersed in HCl to selectively remove the InP substrate, stopping at the InGaAs layer [23]. The thin-film MSM mesa devices in the Apiezon W wax were then bonded to a mylar transfer diaphragm. The Apiezon W was dissolved with trichloroethylene, leaving the thin-film MSM PD devices bonded to the mylar transfer diaphragm. The final thickness of the MSM thin-film devices was 0.9  $\mu\text{m}$ .

When the MSMs are bonded to the interconnection substrate, they are inverted, thus forming I-MSMs. I-MSMs have a higher surface normal responsivity than conventional MSMs since the finger shadowing is eliminated [23]–[25]. MSMs have larger area per unit capacitance than PIN devices at the same speed (for frequencies over approximately 500 MHz), which make them attractive for high speed operation in waveguide interconnection system. For example, transimpedance amplifier interface circuits (TIAs) operate with limited input capacitance from PDs, and, as speeds rise, PD areas decrease. Thus, to ensure adequate input signal to the TIA, large area (i.e., more coupled signal), low capacitance PDs are essential. At very high data rates (100 Gb/s), the coupling efficiency will be limited by the waveguide/PD interaction length, so maximizing PD size for a

given capacitance is essential. An optimized interconnect integration using I-MSMs and polymer optical waveguides can offer high speed, high responsivity operation with large area PDs coupled with low capacitance.

Next, the Si interconnection substrates were prepared for the integration of the optical interconnect. For the first integration structure, as shown in Fig. 2(d), a 3- $\mu\text{m}$  layer of  $\text{SiO}_2$  was deposited onto the Si substrate using plasma enhanced chemical vapor deposition (PECVD). Electrical contact pads of Ti–Au (400 Å/5000 Å) were deposited and patterned on this substrate. For the second integration structure, as shown in Fig. 2(e), the thin-film MSM photodetector was bonded on top of a 1- $\mu\text{m}$  BCB core layer, which is on top of a 3- $\mu\text{m}$  layer of  $\text{SiO}_2$  deposited using PECVD. The 1- $\mu\text{m}$ -thick BCB core layer was spin coated onto the  $\text{SiO}_2$ , followed by a cure at 240 °C for 1 h. Again, electrical contact pads of Ti–Au (400 Å/5000 Å) were deposited and patterned on this substrate. The third integration structure [Fig. 2(f)] process starts with depositing electrical contact pads of Ti–Au (400 Å/5000 Å) on a 3  $\mu\text{m}$   $\text{SiO}_2$  optical buffer layer on a Si substrate.

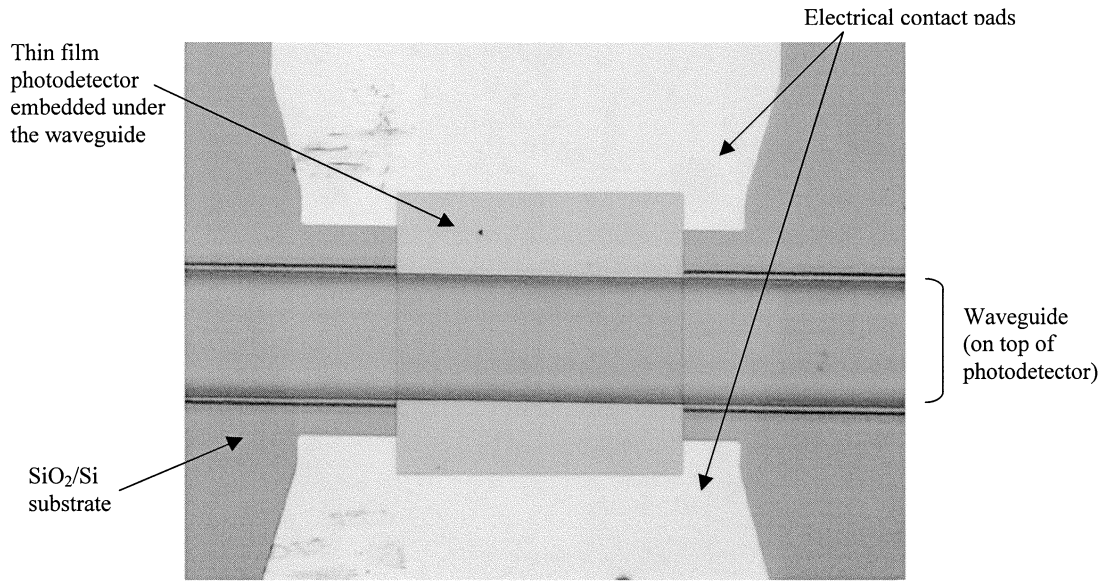
Next, for all three samples, thin-film MSMs were transferred onto the metallized contact pads on the Si substrate, and subsequent waveguide layers were deposited. The MSMs were transferred using a mylar transfer diaphragm [24], [25], and were bonded to metallized pads on the substrates, thus inverting the MSM photodetector (creating the I-MSM). This metal (I-MSM pad) to metal (Si substrate pad) bond is an electrically conducting, mechanically stable bond formed using a low temperature thermal anneal of 10 minutes at 150 °C, which was performed after the device was bonded to the contact pads. The waveguide fabrication process was then continued to embed the photodetector in a BCB waveguide [as in Fig. 2(d) and (e)], and in a BCB cladding with an Ultem core [as in Fig. 2(f)]. For Fig. 2(d), BCB (Cyclotene 3022-57) was spin coated onto the I-MSM/ $\text{SiO}_2$ /Si substrate at 5000 rpm for 30 s and cured to create the waveguide core layer, resulting in a thickness of 6  $\mu\text{m}$ . To minimize additional loss due to the surface step caused by the 0.9- $\mu\text{m}$ -thick I-MSM PD, the BCB core layer was chemi-mechanically polished (CMP) using Rodel 3116B and deionized water. The abrasive used for the slurry was 0.05- $\mu\text{m}$   $\text{Al}_2\text{O}_3$ . The final thickness and surface roughness of the core layer were 4.3  $\mu\text{m}$ , and 600 Å, respectively, as measured by a profilometer. For the structure shown in Fig. 2(e), the integration process started with spin coating a 6- $\mu\text{m}$ -thick BCB layer onto the I-MSM/BCB/ $\text{SiO}_2$ /Si sample. The total thickness of the BCB core layer (including the layer under the I-MSM) was  $\sim 7$   $\mu\text{m}$  thick. After the CMP, the final core (BCB) thickness was 6.3  $\mu\text{m}$ . The 3- $\mu\text{m}$ -thick  $\text{SiO}_2$  layer was used as a waveguide cladding layer for the two integration structures shown in Fig. 2(d) and (e). For the third integration process [in Fig. 2(f)], the 2.4  $\mu\text{m}$  thick BCB was spin coated onto the I-MSM/ $\text{SiO}_2$ /Si sample to form the cladding layer, and was cured. Then the sample was chemically–mechanically polished, as in the previous samples, to a thickness of 1.2  $\mu\text{m}$  (which left 0.2  $\mu\text{m}$  of BCB between the PD and the Ultem core). Then a 1.8- $\mu\text{m}$ -thick Ultem layer was spin coated onto the BCB to create the waveguide core layer. For all three planar waveguide samples, a 100- $\mu\text{m}$ -wide channel were patterned

using a thick photoresist mask and  $\text{SF}_6/\text{O}_2$  reactive ion etching. The width of the fabricated waveguide was designed to match the detection area (100  $\mu\text{m} \times 150 \mu\text{m}$ ) of the embedded I-MSM PD to maximize the coupling efficiency from the waveguide to the embedded I-MSM PD. There are several reasons behind the selection of the size of the PD. First, typical board manufacturers utilize 4 mil lines (100 microns) for board fabrication, and this first demonstration was focused upon not high-speed performance, but upon a demonstration of a technology which is integrable with current board manufacturing technology, as this research is designed for transfer to printed wiring boards such as high temperature FR4. A second reason was to demonstrate a high coupling efficiency for this first demonstration. In future research, we plan to refine the structure and size of the waveguide/PD design to optimize for coupling efficiency as a function of interconnect bandwidth.

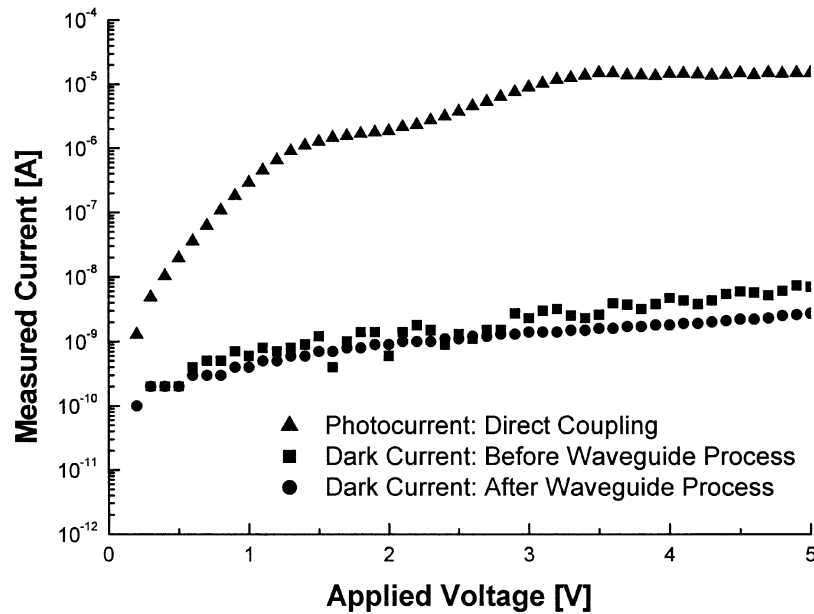
Photomicrographs of the fabricated I-MSM PDs embedded in the fabricated polymer waveguides on the Si substrates are shown in Figs. 3(a), 4(a), and 5(a). The two direct coupling integration structures (BCB/PD/ $\text{SiO}_2$ /Si, and BCB/PD/BCB/ $\text{SiO}_2$ /Si) are shown in Figs. 3(a) and 4(a), respectively. In Fig. 5(a), the embedded detector in the cladding (BCB) for the Ultem/BCB/PD/ $\text{SiO}_2$ /Si structure is shown. For all three embedded structures, the dimensions of the fabricated thin-film I-MSM PDs and the contact pads on the substrates were the same.

### III. CHARACTERIZATION OF THE I-MSM PDs EMBEDDED IN THE POLYMER WAVEGUIDES

The I-MSM dark current and photoresponse were measured before and after waveguide integration. The dark current and photoresponse of the I-MSMs were measured using a Keithley 238 source measurement unit to measure the output current of the I-MSMs. A single-mode pigtailed laser diode fiber output was connected to a 62.5  $\mu\text{m}$  multimode fiber, and this was used as the optical input for the surface normal I-MSM responsivity measurements. The measured optical output power from the pigtailed laser diode was 1.5 mW at a wavelength of 1.3  $\mu\text{m}$ . The I-MSM surface normal responsivity was measured before the waveguide was integrated onto each detector, and, without an AR coating, all of the I-MSMs had a measured responsivity of 0.38 A/W at 5 V. After the waveguide integration, to test the waveguide coupling, each Si substrate was cleaved to produce an endface on the polymer waveguide, and a single-mode optical fiber [core diameter = 9  $\mu\text{m}$ , numerical aperture (NA) = 0.13] was endface coupled to each polymer waveguide. Figs. 3(b), 4(b), and 5(b) show the measured dark current before and after the polymer optical waveguide process, as well as the photocurrent due to the coupling from the waveguide to the I-MSM PD embedded in the waveguide. The measured dark current for all of the embedded PDs decreased slightly after the polymer waveguide integration process, as shown in Figs. 3(b), 4(b), and 5(b), due to the use of the low temperature anneal coupled with the Pt–Ti–Pt–Au Schottky contact. The measured photocurrents at 5V for the three different coupling structures were 15.02  $\mu\text{A}$  [direct coupling shown in Fig. 3(b)], 42.02  $\mu\text{A}$  [direct coupling shown in Fig. 4(b)], and 0.80  $\mu\text{A}$  [evanescent field coupling shown in Fig. 5(b)]. These experiments show that the optical



(a)



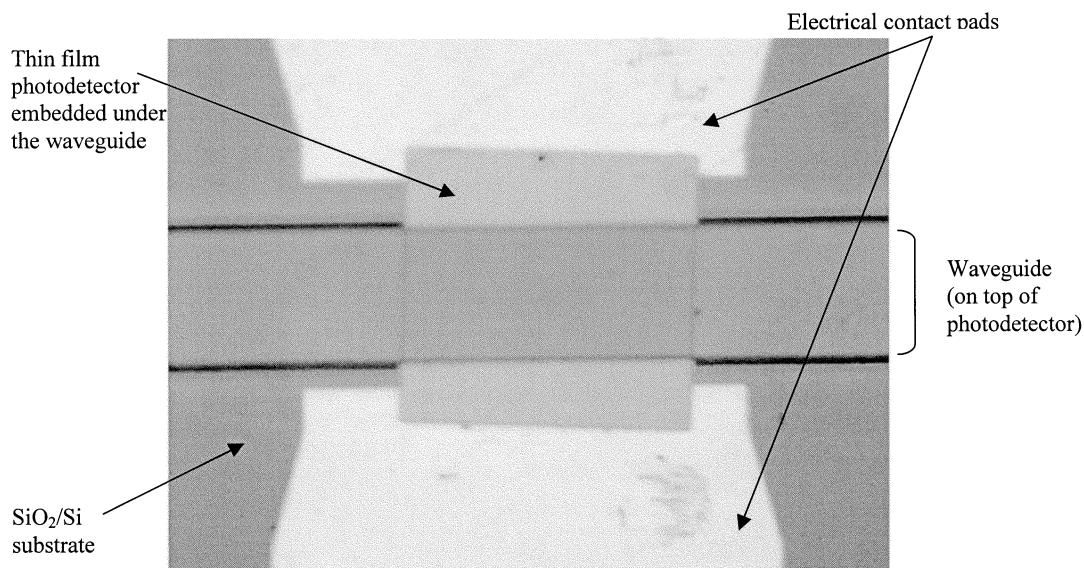
(b)

Fig. 3. (a) Photomicrograph of a thin-film I-MSM photodetector embedded in a polymer waveguide ( $4.3 \mu\text{m}$  BCB/PD/ $3 \mu\text{m}$  SiO<sub>2</sub>) on a Si electrical interconnection substrate. The associated schematic is Fig. 2(d); (b) measured dark current before and after waveguide integration and photocurrent from the embedded I-MSM PD shown in Fig. 3(a).

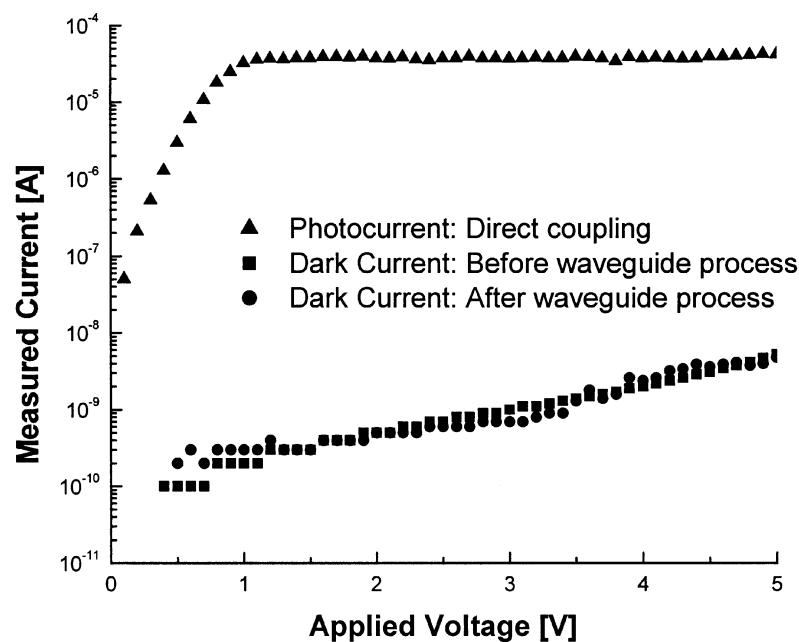
signal in the waveguide has been successfully coupled into the embedded photodetector. In Section V, the demonstrated coupling efficiency and a characterization of the coupling efficiency for these structures are explored theoretically.

The propagation loss of the integrated channel polymer waveguides was measured using the optical fiber scanning method [17]. The probing large core multimode fiber (core diameter =  $600 \mu\text{m}$ , NA = 0.37) measures the scattered optical signal from each channel waveguide. The probing optical fiber was set at the same height (within a centimeter) from the sample while 300 scanning points (using a Coherent motorized micropositioner) were measured perpendicular to the waveguide in  $10 \mu\text{m}$  increments. These 300 points constitute one scan line, and there were 300 scan lines measured, with each line separated by  $10 \mu\text{m}$ . The propagation loss per unit

distance was calculated by the slope of the linear least square regression line of the average collected (scattered) optical power from each waveguide before the detector, as measured through the probing large core optical fiber. This measurement assumes uniform scattering along the fabricated optical channel waveguide. Using this method, the estimated propagation loss of the multimode BCB polymer channel waveguide was 0.36 dB/cm at a wavelength of  $1.3 \mu\text{m}$ . This estimate includes intrinsic material, structural, and other possible propagation loss sources of the polymer optical waveguide, which is consistent with other reported results for BCB waveguides [27], [28]. For the Ultem/BCB channel waveguide shown in Fig. 5(a), the propagation loss at  $\lambda = 1.3 \mu\text{m}$  was measured using the fiber scanning method. The scanning condition for the perpendicular direction to waveguide beam propagation was 100 points with



(a)



(b)

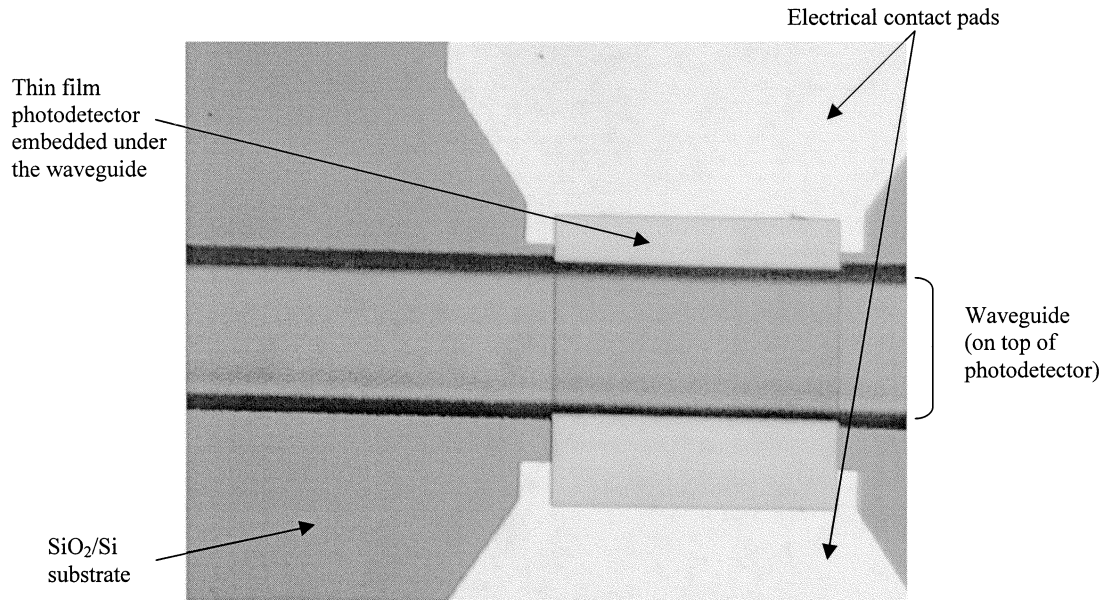
Fig. 4. (a) Photomicrograph of a thin-film I-MSM photodetector embedded in a polymer waveguide (5.3- $\mu\text{m}$  BCB/PD/1  $\mu\text{m}$  BCB/3- $\mu\text{m}$  SiO<sub>2</sub>) on a Si electrical interconnection substrate. The associated schematic is Fig. 2(e); (b) measured dark current before and after waveguide integration and photocurrent from the embedded I-MSM PD shown in Fig. 4(a).

50  $\mu\text{m}$  increments in a scan line. This perpendicular scan line was repeated for a 1 cm length along the waveguide with 100  $\mu\text{m}$  line separations. Using this measurement, the estimated propagation loss for the Ultem/BCB channel waveguide was 1.34 dB/cm. To our knowledge, this is the first reported channel waveguide loss for Ultem/BCB at  $\lambda = 1.3 \mu\text{m}$ . Planar slab waveguide measurements of Ultem at  $\lambda = 850 \text{ nm}$  indicate a loss of 0.3 dB/cm [29].

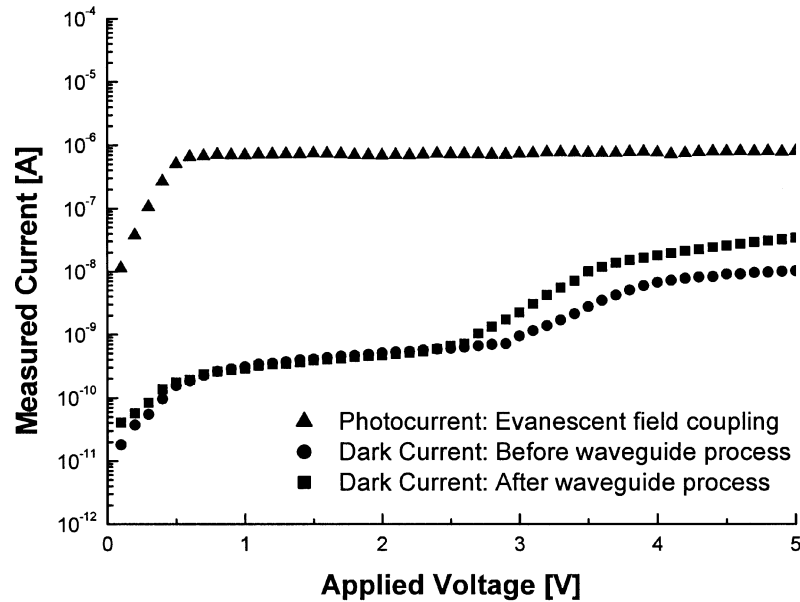
#### IV. DESIGN CONSIDERATIONS FOR EMBEDDED PHOTODETECTORS IN POLYMER WAVEGUIDES

Several theoretical analysis approaches have been suggested for photodetectors monolithically integrated with optical

waveguides [30]–[32]. Although the integrated structured described herein is not monolithic, these methods are also applicable for modeling the thin-film PDs embedded in waveguides, as discussed herein. One of the most commonly used analysis methods for integrated waveguide/photodetector structures is the beam propagation method (BPM) [33]–[35]. However, there are some restrictions associated with the conventional BPM method when modeling high index contrast in the structure and reflected traveling beams. In the models presented herein, the high index contrast problem between the polymer optical waveguides and the embedded photodetectors and the possible reflections at the interfaces between the input waveguide regions and the embedded regions were addressed with wide angle and bidirectional BPM, using the same



(a)



(b)

Fig. 5. Photomicrograph of a thin-film I-MSM photodetector embedded in a polymer waveguide ( $1.8 \mu\text{m}$  Ultem/ $0.2\text{-}\mu\text{m}$  BCB/PD/ $3\text{-}\mu\text{m}$   $\text{SiO}_2$ ) on a Si electrical interconnection substrate. The associated schematic is Fig. 2(f); (b) measured dark current before and after waveguide integration and photocurrent from the embedded I-MSM PD shown in Fig. 5(a).

approach as other reports in the literature with similar issues [36], [37]. In the thin-film photodetector/waveguide integration structure, the coupling efficiency as a function of integration structure is one of the important design issues for the optimized optical signal distribution in the interconnection system. In this calculation, the 2-D scalar finite difference beam propagation method (FD-BPM) from a commercial software package, Rsoft, was used. The detector length was fixed at  $150 \mu\text{m}$  and the real and imaginary parts of the refractive index [38] for InGaAs lattice matched to InP was used as the detector region.

In the direct coupling scheme, the photodetector was integrated into the core layer of the optical waveguides, as shown in Fig. 2(d) and (e). Fig. 6(a) and (b) show the direct coupling efficiencies from the waveguide into the embedded MSM pho-

todetector, which are schematically shown in Fig. 2(d) and (e), respectively, as a function of the total thickness of the BCB (core) layer at a  $\lambda = 1.3 \mu\text{m}$ . In the calculation for Fig. 6(b), the embedded photodetector is located on top of  $1\text{-}\mu\text{m}$ -thick BCB, above the top of the  $\text{SiO}_2$  (cladding) layer, which is based on the fabricated structure. As shown in Fig. 6(a) and (b), the amount of optical power coupled into the embedded photodetector can be optimally selected by changing the location of the embedded photodetector in the waveguide.

In the evanescent field coupling scheme, the photodetector was integrated into the cladding layer of the optical waveguide, as shown in Fig. 2(f). Fig. 6(c) and (d) show the calculated evanescent field coupling efficiencies for different thicknesses of the core layer [Ultem, Fig. 6(c)] and cladding

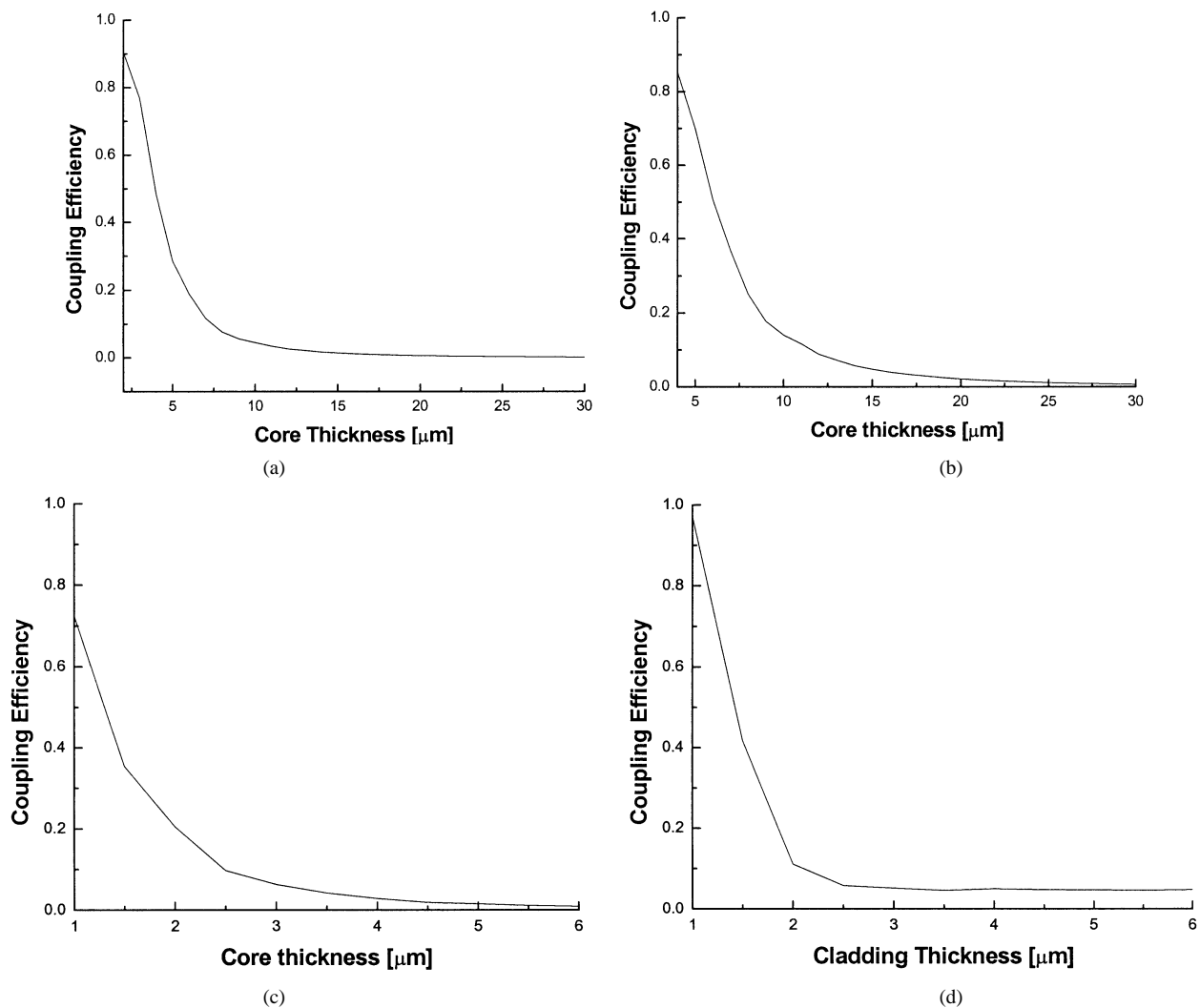


Fig. 6. Theoretical coupling efficiency as a function of integration structure. (a) Coupling efficiency as a function of core (BCB) thickness with an embedded I-MSM PD on the bottom of core layer, as schematically shown in Fig. 2(d); (b) coupling efficiency as a function of core (BCB) thickness with an embedded I-MSM PD  $1\ \mu\text{m}$  above the bottom of core layer, as schematically shown in Fig. 2(e); (c) coupling efficiency as a function of core (Ultem) thickness with an embedded I-MSM PD on the bottom of a  $1.2\text{-}\mu\text{m}$ -thick cladding (BCB) layer, as schematically shown in Fig. 2(f); (d) coupling efficiency as a function of cladding (BCB) thickness with an embedded I-MSM PD on the bottom of the cladding (BCB) layer, with a  $1\text{-}\mu\text{m}$ -thick Ultem core, as schematically shown in Fig. 2(f).

[BCB, Fig. 6(d)], as schematically shown in Fig. 2(f). In the evanescent field coupling case, a major factor that affects the coupling efficiency is the separation between the embedded PD and the core layer (i.e., the thickness of the BCB cladding layer between the PD and the Ultem core). For Fig. 6(c), the thickness of the cladding layer between the PD and the Ultem core was fixed at  $0.2\ \mu\text{m}$  (based upon the experimental sample). The coupling efficiency is inversely proportional to the thickness of the core layer. For Fig. 6(d), the Ultem core layer was fixed at a  $1\ \mu\text{m}$  thickness, and the BCB cladding thickness varied. Again, the coupling efficiency is inversely proportional to the cladding thickness. As this cladding thickness and the core layer thickness increase, the overlap area of the propagating optical mode distribution and embedded photodetector is decreased.

#### V. EMBEDDED STRUCTURE COUPLING EFFICIENCY THEORETICAL CHARACTERIZATION

The coupling from the waveguides to the PDs can be modeled and estimated, but it is difficult to precisely measure

the coupling for the embedded PDs due to the difficulty in estimating the fiber to waveguide endface coupling efficiency. Using the BPM theory described in the previous section, the waveguide to I-MSM coupling efficiency was theoretically calculated, and now, a comparison of the theoretical coupling efficiency will be made to the coupling that is estimated from the measurement results. First, the single-mode fiber endface coupling into the fabricated waveguide structures was estimated using BPM. Then the measured propagation loss of the fabricated waveguide is taken into account to calculate the amount of optical power that is incident on the embedded detector. For example, the measured output from the single-mode optical fiber was  $1.56\ \text{mW}$  in the experimental measurement of the embedded photodetector sample shown in Fig. 3(a). Using BPM, the estimated optical power from a single-mode input optical fiber with a  $9\text{-}\mu\text{m}$ -thick core to the  $100\text{-}\mu\text{m}$ -wide and  $4.3\text{-}\mu\text{m}$  BCB/ $3.0\text{-}\mu\text{m}$   $\text{SiO}_2$  waveguide was  $193.13\ \mu\text{W}$ , which corresponds to 12.38% of the output power from the optical fiber. The optical signal travels 5 mm from the fiber input to the detector, which causes a loss

of 0.18 dB from the measured propagation loss. Thus, the estimated optical power incident on the embedded detector in the waveguide is 185.29  $\mu\text{W}$ . To calculate the PD absorbed optical power, the photocurrent (15.02  $\mu\text{A}$ ) from the embedded photodetector (when it is excited through coupling in the waveguide) is divided by the PD surface normal responsivity (0.38 A/W). Thus, 39.53  $\mu\text{W}$  of optical power was absorbed by the photodetector. So, the estimated coupling efficiency is the absorbed power divided by the incident power, which is 21.33%. This does not take into account the reflection and scattering loss at the waveguide/PD interface, which will increase the estimated coupling efficiency. The theoretical coupling efficiency from the 4.3- $\mu\text{m}$  BCB/3.0- $\mu\text{m}$  SiO<sub>2</sub> waveguide into the 150- $\mu\text{m}$ -long embedded I-MSM PD was 33.78% using scalar BPM analysis. The calculated reflection and scattering loss at the waveguide/PD interface was 5.51% by the same analysis. This estimate included the following inputs: waveguide BCB index of refraction = 1.53 at  $\lambda = 1.3 \mu\text{m}$  (based upon the BCB vendor data for the deposition conditions used), SiO<sub>2</sub> index of refraction = 1.45 at  $\lambda = 1.3 \mu\text{m}$  (based upon the PECVD data for the deposition conditions used), fiber core refractive index = 1.5, diameter = 9  $\mu\text{m}$ . The fiber optical excitation mode is assumed to be a fundamental fiber mode that matches the fiber core diameter. The experimentally estimated coupling efficiency was 9.39% for the evanescent field coupling structure shown in Fig. 5(a) (1.8  $\mu\text{m}$  Ultem waveguide with index of refraction = 1.65 at  $\lambda = 1.3 \mu\text{m}$ /1.2  $\mu\text{m}$  BCB), compared to a theoretical coupling efficiency of 19.80%. The calculated loss at the interface by reflection and scattering was 1.31% for Ultem/BCB structure. The difference between the theoretical and experimental estimated coupling efficiencies may be affected by several factors. The dominant factor that may affect the estimates of the coupling efficiency is the uncertainty and nonuniformity of the waveguides in the region of the embedded photodetector. As illustrated in Fig. 6, small changes in the waveguide thickness can cause large changes in the coupling efficiency.

Although this estimate of the measured coupling efficiency is very rough, it does indicate that sufficient coupling can be achieved to create a viable interconnect. One of the attractive aspects of this integration technology is that the coupling can be intentionally varied through structural design so that the majority of the optical signal can be detected, or a fraction of the signal can be detected, thus enabling subsequent PDs in an array format to be addressed further along the optical path on the same waveguide for spatial-division multiplexing.

## VI. CONCLUSION

As aggregate system data rates rise, significant opportunities are emerging for optical interconnections at the board, module, and chip level if compact, low loss, high data rate optical interconnections can be integrated into electrical interconnection systems. There are numerous approaches to the integration of optical interconnections into electrical systems. This paper describes an embedded integration process for creating optical interconnections which can be integrated in a postprocessing format onto standard boards (including polymer and epoxy),

modules, and integrated circuits, and shows that the coupling efficiency can be adjusted as designed by changing the integration structures. These optical interconnections utilize active thin-film optoelectronic components embedded in the waveguide/interconnection substrate, thus providing an electrical output to the user from an embedded optical interconnection. These embedded optical interconnections are reported herein using BCB polymer optical waveguides in two different formats, as well as a third waveguide structure using a BCB cladding with an Ultem core. All of these waveguides were fabricated with InGaAs-based thin-film I-MSM photodetectors embedded in the waveguide layer, thus eliminating the need for beam turning elements at the output of the waveguide. These embedded interconnections have been fabricated and tested, and the measured results used to estimate the coupling of the optical signals from the waveguides to the embedded photodetectors. These measurement-based estimates are then compared to theoretical models of the coupling efficiency. Using the theoretical coupling efficiency model, variable coupling can be engineered into the interconnect design, thus enabling partial coupling for arrays of photodetectors embedded in waveguide interconnections.

Using the heterogeneous integration techniques described herein, it is possible to fabricate both directly coupled and evanescently coupled structures using embedded PDs. The coupling efficiency of these structures is variable through the design of the embedded PD in the waveguide, and an analysis of the tradeoffs between direct and evanescent coupling for a fixed PD has been presented herein. One limitation on the coupling efficiency is the back reflection of the guided optical beam at the PD, which is inversely proportional to the overlap area between the guided optical signal in the optical waveguide and the embedded PD. The integration structures with an embedded PD located in the waveguide cladding layer, as shown in Fig. 2(f) and (g), which are evanescently coupled, offer higher coupling efficiency compared to the direct coupled structures, as shown in Fig. 2(d) and (e), for a given size of embedded PD. Thus, the reduction in back reflection is an advantage for the evanescently coupled structure. However, as the speed of the interconnection rises, the directly coupled structures may provide superior performance compared to evanescently coupled structures for two reasons. First, the incident optical signal overlap the highest electric field region in the PD if it is directly coupled, therefore generating carriers in the PD which will have a higher carrier velocity than the evanescently coupled structure. Second, as the speed of the interconnect rises, the size of the PD will shrink, thus reducing the optical interaction length, thus limiting the coupling efficiency. Since the optical power distribution of the guided mode overlap with the PD for the direct coupled structure is larger than that of the evanescently coupled structure, the direct coupled structure may provide an overall larger coupling efficiency for a very short PD. Thus, there is promise for the inclusion of high performance, high complexity optical interconnections with standard electrical signals at the board, module, and integrated circuit level.

## ACKNOWLEDGMENT

The authors would like to thank the National Science Foundation Electronic Packaging Research Center and the State of Georgia Yamacraw Program for their support of this work, and the staff of the Georgia Tech Microelectronics Research Center cleanroom for their support.

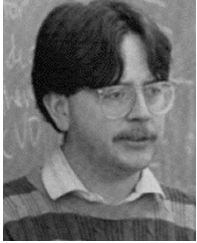
## REFERENCES

- [1] W. J. Dally and J. Poulton, "Transmitter equalization for 4-Gbps signaling," *IEEE Micro*, pp. 48–56, Jan./Feb. 1997.
- [2] C. Yoo, "High-speed DRAM interface," *IEEE Potentials*, vol. 20, pp. 33–34, Dec. 2001/Jan. 2002.
- [3] E. D. Kyriakis-Bitzaros, N. Haralabidis, M. Lagadas, A. Georgakilas, Y. Moisiadis, and G. Halkias, "Realistic end-to-end simulation of the optoelectronic links and comparison with the electrical interconnections for system-on-chip applications," *J. Lightwave Technol.*, vol. 19, pp. 1532–1542, 2001.
- [4] K. A. Jenkins and J. P. Eckhardt, "Measuring jitter and phase error in microprocessor phase-locked loops," *IEEE Des. Test Comp.*, vol. 17, pp. 86–93, Apr.–June 2000.
- [5] M. Horowitz, C.-K. Ken Yang, and S. Sidiropoulos, "High-speed electrical signaling: Overview and limitations," *IEEE Micro*, pp. 12–24, Jan.–Feb. 1998.
- [6] W. Ryu, J. Lee, H. Kim, S. Ahn, N. Kim, B. Choi, D. Kam, and J. Kim, "RF interconnect for multi-Gbit/s board-level clock distribution," *IEEE Trans. Adv. Packag.*, vol. 23, pp. 398–407, 2000.
- [7] D. A. B. Miller, "Rationale and challenges for optical interconnects to electronic chips," *Proc. IEEE*, vol. 88, pp. 728–749, June 2000.
- [8] S. K. Tewksbury and L. A. Hornak, "Optical clock distribution in electronic systems," *J. VLSI Signal Processing*, vol. 16, pp. 225–246, 1997.
- [9] M. Rassaian and M. W. Beranek, "Quantitative characterization of 96.5Sn3.5Ag and 80Au20Sn optical fiber solder bond joints on silicon micro-optical bench substrates," *IEEE Trans. Adv. Packag.*, vol. 22, pp. 86–93, 1999.
- [10] S. J. Walker and J. Jahns, "Optical clock distribution using integrated free-space optics," *Opt. Commun.*, vol. 90, pp. 359–371, 1992.
- [11] P. J. Delfyett, D. H. Hartman, and S. Z. Ahmad, "Optical clock distribution using a mode-locked semiconductor laser-diode system," *J. Lightwave Technol.*, vol. 9, pp. 1646–1649, 1991.
- [12] L. Yujie, L. Lei, C. Chulchae, B. Bipin, and R. T. Chen, "Optoelectronic integration of polymer waveguide array and metal-semiconductor-metal photodetector through micromirror couplers," *IEEE Photon. Technol. Lett.*, vol. 13, pp. 355–357, Apr. 2001.
- [13] S. M. Schultz, E. N. Glytsis, and T. K. Gaylord, "Volume grating preferential-order focusing waveguide coupler," *Opt. Lett.*, vol. 24, pp. 1708–1710, 1999.
- [14] N. M. Jokerst, M. A. Brooke, J. Laskar, D. S. Wills, A. S. Brown, M. Vrazel, S. Jung, Y. Joo, and J. J. Chang, "Microsystem optoelectronic integration for mixed multisignal systems," *IEEE J. Select. Topics Quantum Electron.*, vol. 6, pp. 1231–1239, Nov.–Dec. 2000.
- [15] St. Kollakowski, A. Strittmatter, E. Dröge, E. H. Böttcher, and E. H. Bimberg, "65 GHz InGaAs/InAlGaAs/InP waveguide-integrated photodetectors for the 1.3–1.55  $\mu\text{m}$  wavelength regime," *Appl. Phys. Lett.*, vol. 74, pp. 612–614, 1999.
- [16] E. H. Böttcher, H. Pfitzenmaier, E. Dröge, S. Kollakowski, A. Stittmatter, D. Bimberg, and R. Steingrüber, "Distributed waveguide-integrated InGaAs MSM Photodetectors for high-efficiency and ultra-wideband operation," in *Proc. IEEE 11th Int. Conf. Indium Phosphide and Related Materials*, 1999, pp. 79–82.
- [17] R. T. Chen, L. Lin, C. C. Choi, Y. J. Liu, B. Bihari, L. Wu, S. Tang, R. Wickman, B. Picor, M. K. Hibbs-Brenner, J. Bristow, and Y. S. Liu, "Fully embedded board-level guided-wave optoelectronic interconnects," *Proc. IEEE*, vol. 88, pp. 780–793, June 2000.
- [18] C. H. Buchal, A. Roelofs, M. Siegert, and M. Löken, "Polymeric strip waveguides and their connection to very thin ultrafast metal-semiconductor-metal detectors," in *Proc. Mat. Res. Soc. Symp.*, vol. 597, 2000, pp. 97–102.
- [19] F. Gouin, L. Robitaille, C. L. Callender, J. Noad, and C. Almeida, "A 4×4 optoelectronic switch matrix integrating an MSM array with polyimide optical waveguides," *Proc. SPIE*, vol. 3290, pp. 287–295, 1997.
- [20] C. L. Callender, L. Robitaille, J. P. Noad, F. Gouin, and C. Almeida, "Optimization of metal-semiconductor-metal (MSM) photodetector arrays integrated with polyimide waveguides," *Proc. SPIE*, vol. 2918, pp. 211–221, 1997.
- [21] O. Vendier, N. M. Jokerst, and R. Leavitt, "High efficiency inverted GaAs-based MSM Photodetectors," *Electron. Lett.*, vol. 32, no. 4, pp. 394–395, Feb. 1996.
- [22] D. G. Ivey, P. Jian, R. Bruce, and G. Knight, "Microstructural analysis of Au/Pt/Ti contacts to p-type InGaAs," *J. Mater. Sci.: Mater. Electron.*, vol. 6, pp. 219–227, 1995.
- [23] O. Vendier, N. M. Jokerst, and R. P. Leavitt, "Thin-film inverted MSM Photodetectors," *IEEE Photon. Technol. Lett.*, vol. 8, pp. 266–268, Feb. 1996.
- [24] N. M. Jokerst, M. A. Brooke, O. Vendier, S. Wilkinson, S. Fike, M. Lee, E. Twyford, J. Cross, B. Buchanan, and S. Wills, "Thin-film multilayered optoelectronic integrated circuits," *IEEE Trans. Comp., Packag., Manuf. Technol.—Pt. B*, vol. 1, pp. 97–106, Feb. 1996.
- [25] N. M. Jokerst, "Hybrid integrated optoelectronics: Thin film devices bonded to host substrates," *Int. J. High Speed Electron. and Syst.*, vol. 8, pp. 325–356, 1997.
- [26] R. Kirchoff, C. Carriere, K. Bruza, N. Rondan, and R. Sammler, "Benzocyclobutenes: A new class of high performance polymer," *J. Macro. Sci.-Chem.*, vol. 28, pp. 1079–1113, 1991.
- [27] S. Wolff, A. R. Giehl, M. Renno, and H. Fouckhardt, "Metallic waveguide mirrors in polymer film waveguides," *Appl. Phys. B*, vol. 73, pp. 623–627, 2001.
- [28] G. Fischbeck, R. Moosburger, M. Topper, and K. Peterman, "Design concept for singlemode polymer waveguides," *Electron. Lett.*, vol. 32, pp. 212–213, 1996.
- [29] Y. S. Liu, R. J. Wojnarowski, W. A. Hennessy, P. A. Piacente, J. Rowlette, J. Jr, M. Kadar-Kallen, J. Stack, Y. Liu, A. Peczkalski, A. Nahata, and Y. Yardley, "Plastic VCSEL array packaging and high density polymer waveguides for board and backplane optical interconnect," in *Proc. 48th Electron. Comp. Tech. Conf.*, 1998, pp. 999–1005.
- [30] T. Baba and Y. Kokubun, "High efficiency light coupling from antiresonant reflecting optical waveguides to integrated photodetector using an antireflecting layer," *Appl. Opt.*, vol. 29, pp. 2781–2792, 1990.
- [31] R. J. Deri, "Monolithic integration of optical waveguide circuitry with III-V photodetectors for advanced lightwave receivers," *J. Lightwave Technol.*, vol. 11, pp. 1296–1313, Aug. 1993.
- [32] E. M. Wright, R. J. Hawkins, and R. J. Deri, "Coupled-mode theory of vertically integrated impedance-matched waveguide/photodetectors," *Opt. Commun.*, vol. 117, pp. 170–178, 1995.
- [33] M. Siegert, M. Loken, C. Glingener, and C. Buchal, "Efficient optical coupling between a polymeric waveguide and an ultrafast silicon MSM Photodiode," *IEEE J. Select. Topics Quantum Electron.*, vol. 4, pp. 970–974, Nov.–Dec. 1998.
- [34] J. F. Vinchant, F. Mallecot, D. Decoster, and J. P. Vilcot, "Photodetectors monolithically integrated with optical waveguides: Theoretical and experimental study of absorbing layer effects," *Proc. Inst. Elect. Eng.*, vol. 136, pp. 72–75, 1989.
- [35] M. C. Amann, "Analysis of a PIN photodiode with integrated waveguide," *Electron. Lett.*, vol. 23, pp. 895–897, 1987.
- [36] R. Scarmozzino, A. Gopinath, R. Pregla, and S. Helfert, "Numerical techniques for modeling guided-wave photonic devices," *IEEE J. Select. Topics Quantum Electron.*, vol. 6, pp. 150–162, Jan.–Feb. 2000.
- [37] G. R. Hadley, "Wide-angle beam propagation using Pade approximant operators," *Opt. Lett.*, vol. 25, pp. 1426–1428, 1992.
- [38] M. Levinshstein and S. Romyantsev, *Handbook Series on Semiconductor Parameters*. Singapore: World Scientific, 1999, ch. 3.



**Sang-Yeon Cho** received the B.S. degree and M.S. in electrical and computer engineering from SungKyunKwan University, Seoul, Korea, in 1997, and 1998, respectively, and the M.S.EE degree from Georgia Institute of Technology, Atlanta, in 2000. He is currently working toward the Ph.D. degree at Georgia Institute of Technology.

His research interest is in high-speed optical interconnection using thin-film active OE devices with polymer optical waveguides.



**Martin A. Brooke** (S'85–M'86) received the B.E. (Elect.) degree (first class honors) from Auckland University, Auckland, New Zealand, in 1981, and the M.S. and Ph.D. degree in electrical engineering from the University of Southern California, Los Angeles, in 1984, and 1988, respectively.

He is currently Associate Professor of Electrical Engineering at The Georgia Institute of Technology. His expertise is in high-speed high-performance signal processing. Current projects include: learning neural network hardware development; neural

network prediction of turbulent flow; focal plane image processing hardware development; 1–20 Gb/s digital CMOS transceiver circuits for low-cost fiber-optic communication; nonlinear filtering algorithms for telecommunications; nonlinear analog to digital converter design; accurate modeling of high-speed circuit parasitics; and statistically relevant device models for accurate prediction of high-performance integrated circuit yield. He holds four U.S. patents. He has published more than 100 articles in technical Journals and Proceedings, and articles on his work have appeared in several trade publications.

Prof. Brooke won a National Science Foundation Research Initiation Award in 1990, and the 1992 IEEE Midwest Symposium on Circuits and Systems, Myril B. Reed Best Paper Award.



**Nan Marie Jokerst** (S'83–M'88–SM'98–F'02) received the Ph.D. degree from the University of Southern California, Los Angeles, in 1989.

She is the Joseph M. Pettit Professor of Optoelectronics in the School of Electrical and Computer engineering at the Georgia Institute of Technology (Georgia Tech.), Atlanta. She joined the Electrical Engineering faculty, Georgia Tech, in 1989. She is the Optoelectronics Thrust Leader for the Georgia Tech National Science Foundation Engineering Research Center in Electronic Packaging. She has

published and presented over 175 papers, three book chapters, and has three patents awarded and two pending.

Dr. Jokerst received an IEEE Millennium Medal in 2000, is an Optical Society of America Fellow, and has received the Harriet B. Rigas Education Award from the IEEE Education Society, a DuPont Young Faculty Award, a National Science Foundation Presidential Young Investigator Award, Newport Research Award, and three teaching awards, and she was a Hewlett Packard Fellow. She has organized and served on numerous conference committees, and served on the Board of Directors of the Optical Society of America as the Chair of the Engineering Council, and on the IEEE Lasers and Electro-Optic Society (LEOS) Board of Governors as an elected member, and as the Vice President of Conferences for IEEE LEOS. She has also served as the elected Chair, Vice Chair, Secretary, and Treasurer of the Atlanta IEEE Section.